

Corrosion Inhibition of Carbon Steel in 0.5 M HCl Solution Using Cationic Surfactants

A.S. Fouda^{1,*}, Y.A. Elewady¹, H.K. Abd El-Aziz¹ and A.M.Ahmed²

¹ Chemistry Department, Faculty of Science, El -Mansoura University, El-Mansoura-35516, Egypt

² Chemistry Department, Faculty of Science, Alex. University, Egypt

*E-mail: asfouda@mans.edu.eg

Received: 9 October 2011 / *Accepted:* 28 September 2012 / *Published:* 1 November 2012

The corrosion inhibition effect of cationic surfactants, namely: cetyl trimethyl ammonium bromide: CTAB and dodecyl trimethyl ammonium chloride: DTAC, have been used as corrosion inhibitors for C-steel in 0.5 M HCl. The inhibition efficiencies of the tested surfactants were depended on the hydrophobic chain length and the used doses of the surfactants. The results showed that the order of inhibition efficiency is CTAB > DTAC. Polarization measurements showed these surfactants are acting as mixed inhibitors for both anodic and cathodic reactions. Adsorption of these surfactants was found to follow the Langmuir's adsorption isotherm. Mixed physical and chemical adsorption mechanism is proposed. The density function theory (DFT) was used to study the structural properties of the surfactants. Inhibition efficiency values obtained from weight loss, potentiodynamic polarization, electrochemical impedance spectroscopy (IES) and electrochemical frequency modulation (EFM) are consistent.

Keywords: A. Carbon steel, B. Polarization, B. Weight loss, B. EIS, B. EFM, C. Acid corrosion

1. INTRODUCTION

In oil fields, hydrochloric acid solution is recommended as the cheapest way to dissolve calcium carbonate, CaCO₃, scale inside the pipelines under most conditions. Accordingly, corrosion inhibitors (usually surfactants) must be injected with the hydrochloric acid solution to avoid the destructive effect of acid on the surface of the pipe lines [1]. Carbon steel has been widely employed as construction materials for pipe work in the oil and gas production such as down hole tubular, flow lines and transmission pipelines [2]. Surfactants are molecules composed of a polar hydrophilic group, the 'head', attached to a non polar hydrophobic group, the 'tail'. In general, in aqueous solution the inhibitory action of surfactant molecules may also be due to physical (electrostatic) adsorption or chemisorption onto the metallic surface, depending on the charge of the solid surface and the free

energy change of transferring a hydrocarbon chain from water to the solid surface. The adsorption of the surfactants markedly changes the corrosion resisting property of a metal, and for this reason, studies on the relation between adsorption and corrosion inhibition are of considerable importance [3-6]. The adsorption behavior of surfactants at the solid-solution interface is described by many authors [7, 8].

The adsorption occurs due to the interaction of the lone pair and/or π -orbitals of inhibitor with d-orbitals of the metal surface atoms, which evokes a greater adsorption of the inhibitor molecules onto the surface, leading to the formation of a corrosion protection film [9-11].

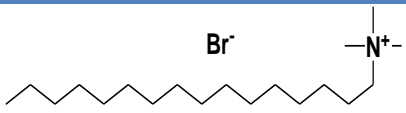
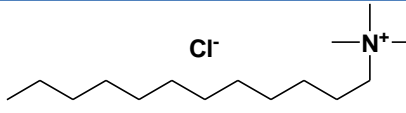
Ionic surfactants have been used for the corrosion inhibition of steel [12-25], copper [26-31], aluminum [32-35] and other metals [36] in different media. Gemini surfactants (cationic surfactants) as corrosion inhibitors for carbon steel pipelines in acidic media have been studied [37-43].

The objective of this work is to study the effect of investigated surfactants on the corrosion inhibition of carbon steel in 1 M HCl solution with electrochemical impedance spectroscopy (EIS), potentiodynamic polarization, electrochemical frequency modulation (EFM) and weight loss measurements methods. In addition we investigated the adsorption mechanism of these inhibitors on carbon steel surface by using Langmuir isotherm. Another objective in this work is to calculate the more relevant molecular properties on its action as corrosion inhibitors.

2. EXPERIMENTAL

2.1. Chemicals and materials

Table 1. Molecular and structure formulae of CTAB and DTAC

Surfactant	Structure formula	Molecular formula	Molecular Weight
CTAB		$C_{16}H_{33}N(CH_3)_3-Br$	364.45
DTAC		$C_{12}H_{25}N(CH_3)_3-Cl$	263.89

Hydrochloric acid (37 %), ethyl alcohol and acetone were purchased from Algamhoria Co.(Egypt). Cetyl trimethyl ammonium bromide (CTAB) and dodecyl trimethyl ammonium chloride (DTAC) were purchased from Aldrich Chemical Company. The molecular and structure formulae of CTAB and DTAC are shown in Table 1. Bidistilled water was used for preparing test solutions for all measurements. The corrosion tests were performed on carbon steel with composition (weight %): C: 0.200, Mn: 0.350, P: 0.024, Si: 0.003 and Fe balance.

2.2. Methods

2.2.1. Weight loss measurements

Rectangular specimens of C-steel with dimensions 2.0 cm x 2.0 cm x 0.2 cm were mechanically abrading with 80, 220, 400, 600, 1000, 1200 grades of emery paper, degreased with acetone, rinsed with bidistilled water and finally dried between filter paper. After weighting accurately, the specimens were immersed in 100 ml of 0.5 M HCl with and without different concentrations of surfactants at 30 °C. After different immersion time (30, 60, 90, 120, 150 and 180 min), the C-steel samples were taken out, washed with bidistilled water, dried between filter papers and weighted again.

The weight loss values are used to calculate the corrosion rate (R) in mm per year by the relation:

$$R = \frac{\text{Wt loss} \times 8.75 \times 10^4}{D \times A \times T} \quad (1)$$

where Wt. loss is weight loss in g, D is the density of carbon steel in g/cm³, A is exposed area in cm², T is exposure time in hr.

The inhibition efficiency (Y_w %) and the degree of surface coverage (Θ) was calculated from:

$$Y_w \% = \theta \times 100 = [(R^* - R) / R^*] \times 100 \quad (2)$$

where R* and R are the corrosion rates of carbon steel in the absence and in the presence of inhibitor, respectively.

2.2.2. Electrochemical measurements

Three electrochemical techniques, namely potentiodynamic polarization, electrochemical impedance spectroscopy (EIS), and electrochemical frequency modulation (EFM), were used to study the corrosion behavior. All experiments were conducted in a conventional three electrodes glass cell. A Pt electrode as counter electrode and a saturated calomel electrode (SCE) as reference electrode were used in this study. The C-steel specimen was machined in to rectangular (1.0 cm x 1.0 cm x 0.3 cm) and sealed with epoxy resin leaving a working area of 1.0 cm². The specimens were polished, degreased and rinsed as described in weight loss measurements.

Potentiodynamic polarization experiments were carried out using a VoltaLab PGZ 100 system connected to personal computer with Volta Master 4 version 7.08 software for calculation. VoltaMaster 4 calculates and displays E_{corr.}, i_{corr.}, β_a, β_c and the corrosion rate (R) in mm per year. All the

experiments were carried out at temperature $(30 \pm 1 \text{ }^\circ\text{C})$. Equilibrium time leading to steady state of the specimens was 30 min and the open circuit potential (OCP) was noted. The potentiodynamic curves were recorded from -900 to -200 mV at a scan rate 2 mV S^{-1} .

The corrosion rate is calculated from the following equation [44]:

$$R = \frac{i_{\text{corr}} \times A \times M}{D \times V} \times 3270 \quad (3)$$

where i_{corr} is the corrosion current density, M is the atomic mass of Fe and V is the valence entered in the Tafel dialogue box.

The $Y_p\%$ was calculated from:

$$Y_p \% = \frac{i_{\text{corr}}^0 - i_{\text{corr}}}{i_{\text{corr}}^0} \times 100 \quad (4)$$

where i_{corr}^0 and i_{corr} are the corrosion current densities of uninhibited and inhibited solution, respectively.

Electrochemical impedance spectroscopy (EIS) and electrochemical frequency modulation (EFM) experiments were carried out using Gamry Instrument Series G 750TM Potentiostat/Galvanostat/ZRA with a Gamry framework system based on ESA400. Gamry applications include software EIS300 for EIS measurements, and EFM140 for EFM measurements to calculate the corrosion current density and the Tafel constants for EFM measurements. A computer was used for collecting data. Echem Analyst 5.5 Software was used for plotting, graphing and fitting data. EIS measurements were carried out in a frequency range of 100 kHz to 100 mHz with amplitude of 5mV peak-to-peak using ac signals at respective corrosion potential. The base frequency was 0.1 Hz. In this study, we use a perturbation signal with amplitude of 10 mV for both perturbation frequencies of 0.2 and 0.5 Hz.

2.2.3. Quantum chemical calculation

Highest occupied molecular orbital energy (E_{HOMO}), Lowest unoccupied molecular orbital energy (E_{LUMO}) and Fukui indices calculations were performed using Materials Studio DMol³ version 4.4.0 [45, 46], a high quality quantum mechanics computer program (available from Accelrys Inc., San Diego, CA). These calculations employed an ab initio, gradient-corrected functional (GGA) method with a double numeric plus polarization (DNP) basis set and a Becke One Parameter (BOP) functional.

It is well-known that the phenomena of electrochemical corrosion appear in aqueous phase. For this reason, it is necessary to include, solvent effect in the computational calculations. In a similar way it is important to take into account the effects that can appear as much in the geometric properties as in the electrical ones. DMol³ includes certain COSMO¹ [47] controls, which allow for the treatment of solvation effects.

3. RESULTS AND DISCUSSION

3.1. Weight loss measurements

Figure 1 shows the weight loss–time curves for the corrosion of C-steel in 0.5 M HCl in the absence and presence of different concentrations of CTAB. Similar curves for DTAC were obtained (not shown).

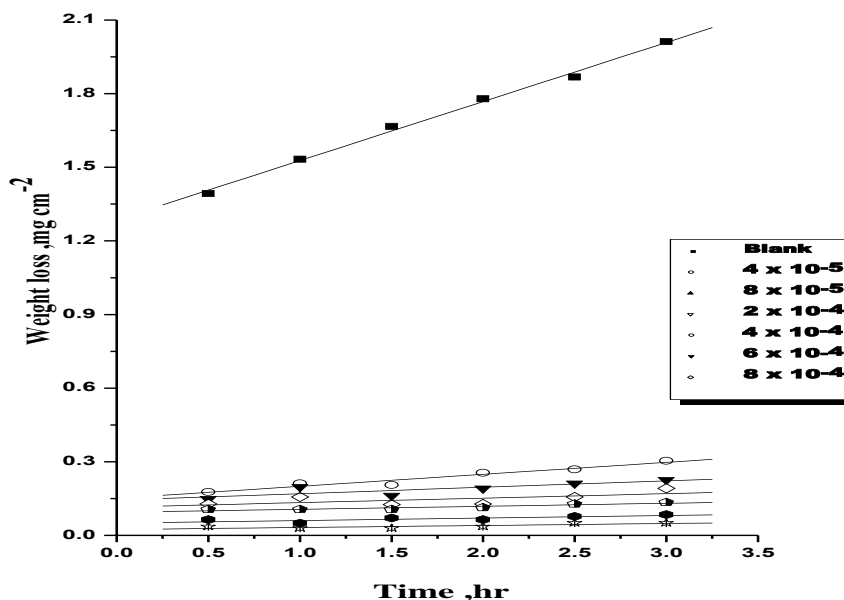


Figure 1. Weight loss-time curves of C-steel in 0.5 M HCl in the absence and presence of different concentrations of CTAB at 30 °C.

Table 2. Data of weight loss measurements for C-steel in 0.5 M HCl solution in the absence and presence of different concentrations of surfactants at 30 °C.

Compound	Conc.,	R (mmy)	θ	Y _w %
Blank	0.00	2.68	-----	-----
DTAC	4.0x10 ⁻⁵	0.80	0.700	70.0
	8.0x10 ⁻⁵	0.56	0.791	79.1
	2.0x10 ⁻⁴	0.39	0.854	85.4
	4.0x10 ⁻⁴	0.35	0.869	86.9
	6.0x10 ⁻⁴	0.22	0.918	91.8
	8.0x10 ⁻⁴	0.19	0.929	92.9
	CTAB	4.0x10 ⁻⁵	0.54	0.799
8.0x10 ⁻⁵		0.29	0.892	89.2
2.0x10 ⁻⁴		0.20	0.925	92.5
4.0x10 ⁻⁴		0.14	0.948	94.8
6.0x10 ⁻⁴		0.12	0.955	95.5
8.0x10 ⁻⁴		0.09	0.966	96.6

The data of Table 2 show that, the dependence of $Y_w\%$ on varying concentration of surfactants (DTAC and CTAB) in the range from 0.04 to 0.8 m mol l^{-1} . It is clear that; at constant temperature the inhibition efficiency increases with increasing the concentration of the surfactant. The lowest corrosion rate is obtained by CTAB therefore $Y_w\%$ tends to decrease in the following order: CTAB > DTAC. The inhibition action of surfactants in HCl cannot be simply considered as an electrostatic adsorption [48] and covalent bonding chemisorption. This action was attributed to the effect of bromide ion of CTAB and chloride ion of DATC. In addition, other factors such as CMC and structure of surfactant might be affecting the inhibition efficiency.

3.2. Electrochemical measurements

3.2.1. Potentiodynamic polarization measurements

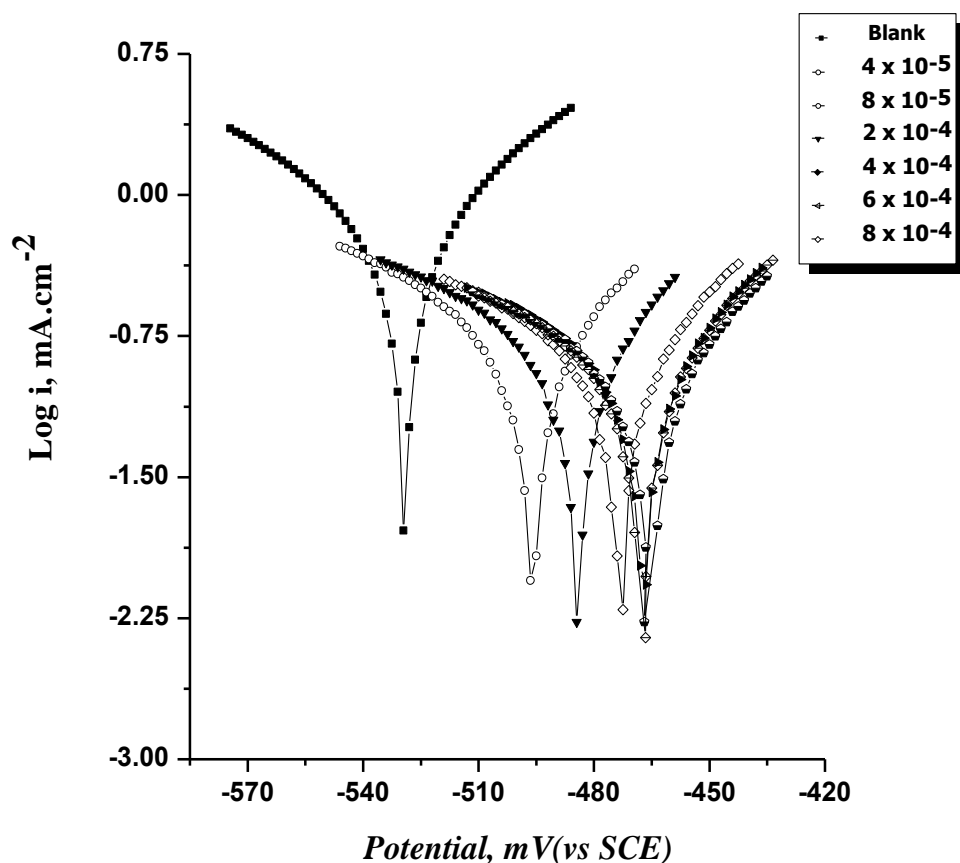


Figure 2. Potentiodynamic polarization for corrosion of C-steel in 0.5 M HCl in the absence and presence of different concentrations of CTAB at 30 °C.

The potentiodynamic curves for C-steel in 0.5 M HCl in the absence and presence of CTAB are shown in Fig.2. Similar curves were obtained for DTAC (not shown). It is clear that; the selected surfactants act as mixed type inhibitors; i.e., promoting retardation of both anodic dissolution of C-

steel and cathodic hydrogen discharge reaction. The i_{corr} values decrease with increasing inhibitor concentration for all inhibitor (Table 3).

Table 3. Potentiodynamic data of C-steel in 0.5 M HCl and in the presence of different concentrations of surfactants at 30 °C.

Compound	Conc., M	-E _{corr} vs. SCE, mV	i_{corr} $\mu\text{A cm}^{-2}$	$-\beta_c$, mV dec^{-1}	β_a , mV dec^{-1}	Θ	$Y_P\%$	R, $\mu\text{m y}^{-1}$
Blank	0	529	515.6	69	54	-----	-----	5976
DTAC	4.0×10^{-5}	518	213.3	75	42	0.586	58.6	2472
	8.0×10^{-5}	502	130.9	78	39	0.746	74.6	1517
	2.0×10^{-4}	477	87.2	82	39	0.831	83.1	1010
	4.0×10^{-4}	472	85.1	79	46	0.835	83.5	994
	6.0×10^{-4}	452	82.3	89	45	0.840	84.0	954
	8.0×10^{-4}	446	69.8	80	45	0.865	86.5	809
	4.0×10^{-5}	501	135.1	79	55	0.738	73.8	1566
CTAB	8.0×10^{-5}	489	126.7	88	53	0.754	75.4	1468
	2.0×10^{-4}	478	86.4	67	44	0.833	83.3	1001
	4.0×10^{-4}	472	79.2	65	43	0.846	84.6	919
	6.0×10^{-4}	470	71.5	64	42	0.861	86.1	828
	8.0×10^{-4}	470	66.8	59	40	0.871	87.1	774

Both cathodic Tafel slopes (β_c) and anodic Tafel slopes (β_a) do not change remarkably, which indicates that the mechanism of the corrosion reaction does not change and the corrosion reaction is inhibited by simple adsorption mode [49]. The irregular trends of β_a and β_c values indicate the involvement of more than one type of species adsorbed on the metal surface. The % IE values were found to decrease as follows (Table 3): CTAB > DTAC. Generally, the increase of the inhibitor concentration shifts corrosion potential into a less negative direction, what can be explained by a small domination of the anodic reaction inhibition.

3.2.2. Electrochemical impedance spectroscopy

The EIS provides important mechanistic and kinetic information for an electrochemical system under investigation. Nyquist impedance plots obtained for the C-steel electrode at respective corrosion potentials after 30 min immersion in 0.5 M HCl in presence and absence of various concentrations of CTAB is shown in Fig.3 (DTAC curves not shown). The Nyquist plots of CTAB do not yield perfect semicircles as expected from the theory of EIS, the impedance loops measured are depressed semi-circles with their centers below the real axis, where the kind of phenomenon is known as the “dispersing effect” as a result of frequency dispersion [50] and mass transport resistant [51] as well as electrode surface heterogeneity resulting from surface roughness, impurities, dislocations, grain boundaries, adsorption of inhibitors, formation of porous layers [52-56], etc. So, one constant phase element (CPE) is substituted for the capacitive element, to explain the depression of the capacitance semicircle, to give a more accurate fit. Impedance data are analyzed using the circuit in Fig.4; in which R_s represents the electrolyte resistance, R_{ct} represents the charge transfer resistance and the constant phase element (CPE).

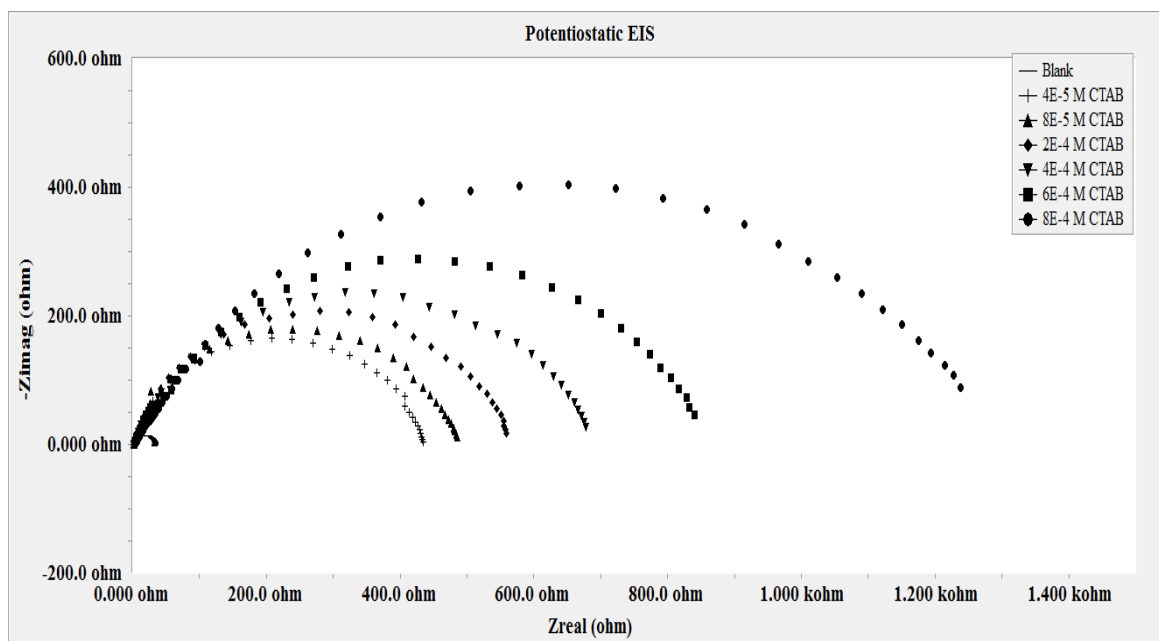


Figure 3. Nyquist plots for C-steel steel in 0.5 M HCl in the different concentrations of CTAB

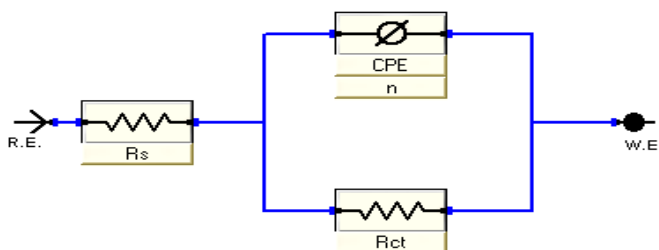


Figure 4. Equivalent circuit model used to fit the impedance spectra

Table 4. EIS data of C-steel in 0.5 M HCl and in the presence of different concentrations of surfactants at 30 °C.

Compound	C_{inh} , M	R_s , $\Omega\text{ cm}^2$	Y , $\mu\Omega^{-1}\text{ s}^n\text{ cm}^{-2}$	n	R_{CT} , $\Omega\text{ cm}^2$	C_{dl} , $\mu\text{F cm}^{-2}$	θ	% Y_1
Blank	0.00	1.946	542.8	0.909	32.1	437	-----	-----
DTAC	4×10^{-5}	1.711	113.1	0.864	187.5	79.4	0.829	82.9
	8×10^{-5}	1.835	73.5	0.849	382.0	48.9	0.916	91.6
	2×10^{-4}	1.794	57.7	0.840	535.3	40.2	0.940	94.0
	4×10^{-4}	1.826	55.3	0.824	637.0	37.2	0.949	94.9
	6×10^{-4}	1.726	53.3	0.757	867.5	36.7	0.963	96.3
	8×10^{-4}	1.473	52.7	0.738	1135.0	36.7	0.972	97.2
CTAB	4×10^{-5}	1.902	80.8	0.871	424.4	61.7	0.924	92.4
	8×10^{-5}	1.982	60.5	0.848	475.2	45.7	0.932	93.2
	2×10^{-4}	2.234	55.5	0.820	559.9	41.8	0.943	94.3
	4×10^{-4}	1.935	38.3	0.781	664.0	27.7	0.952	95.2
	6×10^{-4}	1.989	33.7	0.723	877.7	24.0	0.963	96.3
	8×10^{-4}	1.556	30.4	0.693	1302.0	20.9	0.975	97.5

According to Hsu and Mansfeld [57], the correction of capacity to its real values is calculated from:

$$C_{dl} = Y_o (\omega_{max})^{n-1} \quad (5)$$

where Y_o is the CPE coefficient, ω_{max} is the frequency at which the imaginary part of impedance ($-Z_i$) has a maximum and n is the CPE exponent (phase shift).

The data obtained from fitted spectra are listed in Table 4. The inhibition efficiency (Y_1) and the degree of surface coverage (θ) are calculated from the EIS data by using following equation:

$$Y_1 \% = \theta \times 100 = [(R_{ct} - R_{ct}^*) / R_{ct}] \times 100 \quad (6)$$

where R_{ct} and R_{ct}^* are the charge-transfer resistances with and without the inhibitors, respectively.

Data of Table 4 show that; the R_s values are very small compared to the R_{ct} values. Also; the R_{ct} values increase and the calculated C_{dl} values decrease by increasing the inhibitor concentration, which causes an increase of θ and Y_1 . The high R_{ct} values are generally associated with slower corroding system [51]. The decrease in the C_{dl} suggests that surfactants molecules function by adsorption at the metal/solution interface [58].

The inhibition efficiencies, calculated from EIS, show the same trend as those obtained from polarization and weight loss measurements. The difference of inhibition efficiency from the three methods may be attributed to the different surface status of the electrode in the three measurements. EIS were performed at the rest potential, while in polarization measurements the electrode potential was polarized to high over potential, non-uniform current distributions, resulted from cell geometry, solution conductivity, counter and reference electrode placement, etc., will lead to the difference between the electrode area actually undergoing polarization and the total area [59].

3.2.3. Electrochemical frequency modulation (EFM)

EFM is a nondestructive corrosion measurement like EIS; it is a small signal ac technique. Unlike EIS, however, two sine waves (at different frequencies) are applied to the cell simultaneously. The great strength of the EFM is the causality factors which serve as an internal check on the validity of the EFM measurement [60]. With the causality factors the experimental EFM data can be verified.

The results of EFM experiments are a spectrum of current response as a function of frequency. The spectrum is called the intermodulation spectrum. The spectra contain current responses assigned for harmonical and intermodulation current peaks. The larger peaks were used to calculate the corrosion current density (i_{corr}), the Tafel slopes (β_c and β_a) and the causality factors (CF-2 and CF-3). Intermodulation spectra obtained from EFM measurements are presented in Fig.5 for 0.5 M HCl in absence and presence of 8×10^{-4} M of CTAB and DTAC respectively. Similar curves were obtained

for other concentrations of inhibitors (not shown). Table 5 indicated that; the corrosion current densities decrease by increasing the concentration of the investigated surfactants.

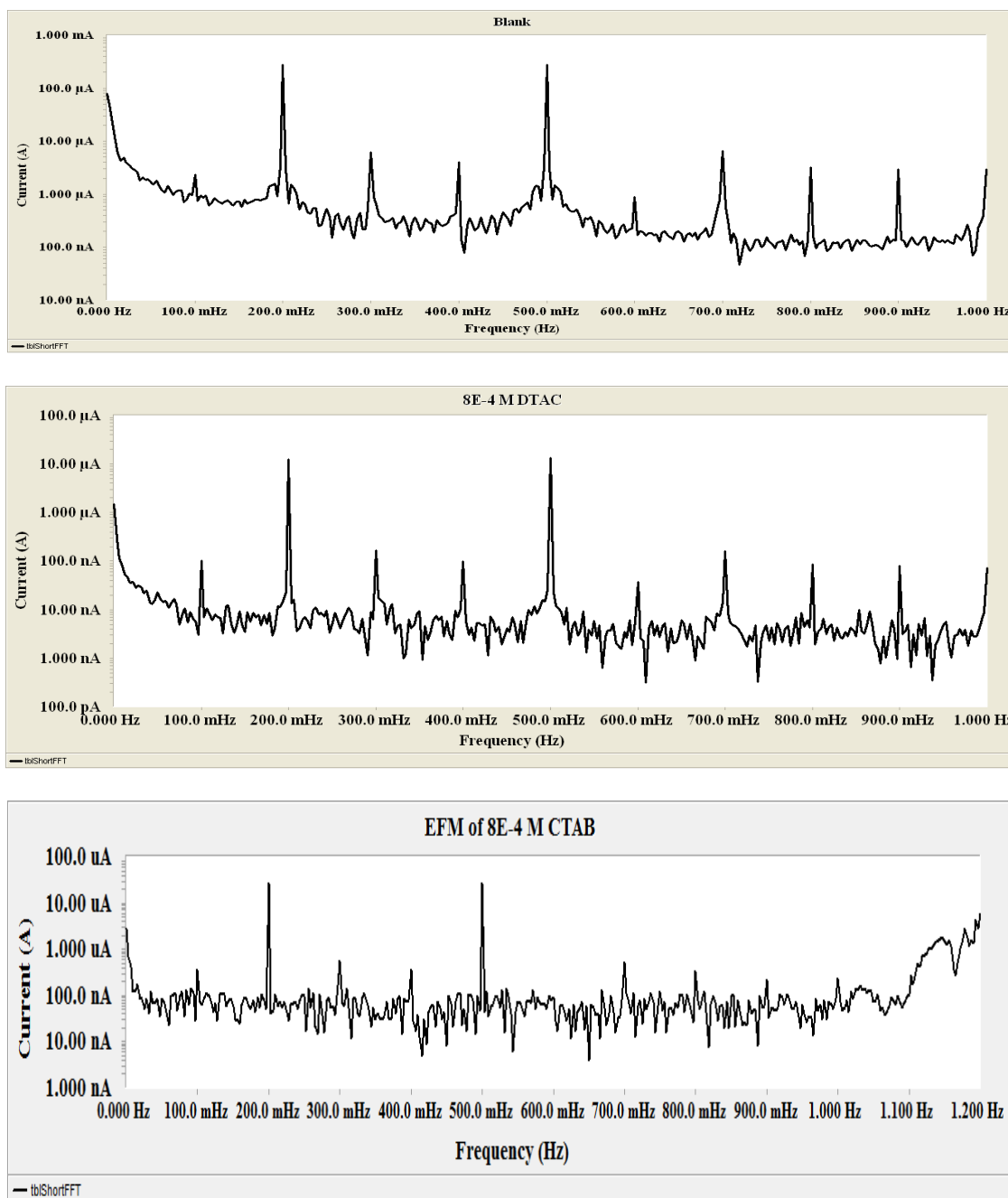


Figure 5. Intermodulation spectra for C-steel in 0.5 M HCl in absence and presence of 8×10^{-4} M concentrations of DTAC and CTAB, respectively.

The inhibition efficiencies, $Y_{EFM}\%$ calculated from Eq. (7) increase by increasing the investigated surfactants concentrations.

$$Y_{EFM} \% = \frac{i_{corr}^0 - i_{corr}}{i_{corr}^0} \times 100 \tag{7}$$

where: i_{corr}^0 and i_{corr} are corrosion current densities in the absence and presence of inhibitors, respectively.

Table 5. Electrochemical kinetic parameters obtained by EFM technique for C- steel in the absence and presence of various concentrations of surfactants in 0.5 M HCl at 30 °C

Compound	Conc., M	i_{corr} $\mu\text{A cm}^{-2}$	β_c mVdec^{-1}	β_a mVdec^{-1}	CF-2	CF-3	CR μm^{-1}	% Y_{EFM}
Blank	0.00	488.9	126	107	1.86	2.95	5763	-----
DTAC	4×10^{-5}	79.10	114	105	1.67	3.01	691	83.8
	8×10^{-5}	42.46	114	106	1.55	3.13	493	91.3
	2×10^{-4}	41.03	132	113	1.91	2.69	476	91.61
	4×10^{-4}	30.79	130	115	2.01	2.77	357	93.7
	6×10^{-4}	28.67	118	113	1.63	2.67	333	94.1
	8×10^{-4}	27.85	150	134	1.91	2.60	323	94.3
CTAB	4×10^{-5}	50.19	121	116	2.10	3.31	0.897	89.7
	8×10^{-5}	41.46	121	112	2.2	3.20	0.915	91.5
	2×10^{-4}	32.34	139	104	1.91	2.80	0.934	93.4
	4×10^{-4}	29.65	127	109	2.09	2.71	0.939	93.9
	6×10^{-4}	21.53	121	115	2.11	2.78	0.956	95.6
	8×10^{-4}	18.66	1240	119	1.80	2.73	0.962	96.2

The causality factors in Table.5 are very close to theoretical values which according to the EFM theory [61] should guarantee the validity of Tafel slopes and corrosion current densities.

3.2.4. Adsorption of surfactants

Adsorption of surfactants on solid surfaces can modify their hydrophobicity, surface charge, and other key properties that govern interfacial processes such as corrosion inhibition [62]. In general, adsorption is governed by a number of forces such as covalent bonding, electrostatic attraction, hydrogen bonding or non-polar interactions between the adsorbed species, lateral associative interaction, solvation, and desolvation [63]. The total adsorption is usually the cumulative result of some or all of the above forces [64].

Standard free energy of adsorption ($-\Delta G_{ads}^\circ$) can be written as [63]:

$$\Delta G_{ads}^\circ = \Delta G_{elec}^\circ + \Delta G_{chem}^\circ + \Delta G_{C-C}^\circ + \Delta G_{C-S}^\circ + \Delta G_H^\circ + \Delta G_{H_2O}^\circ + \dots \tag{8}$$

where ΔG_{elec}° is the electrostatic interaction term, ΔG_{chem}° the chemical term due to covalent bonding, ΔG_{C-C}° the free energy gained upon association of methyl groups in the hydrocarbon chain, ΔG_{C-S}° the free energy due to interactions between the hydrocarbon chains and hydrophobic sites on

the solid, $\Delta G_{\text{H}}^{\circ}$ the hydrogen bonding term and $\Delta G_{\text{H}_2\text{O}}^{\circ}$ is the term owing to dissolution or solvation of the adsorbate species or any species displaced from the interface due to adsorption.

3.2.5. Mechanism of adsorption

The adsorption of ionic surfactants on oppositely charged surface could be taking the following path:

a. At low surfactant concentrations, the adsorption is due to electrostatic interaction between individual isolated charged monomeric species and the oppositely charged solid surface.

b. Surfactant species begin to form surface aggregates, colloids (surface colloids), including hemi-micelles, admicelles, etc., due to lateral interactions between hydrocarbon chains. Due to this additional driving force resulting from the lateral association with the electrostatic interaction still active

c. When the solid surface is electrically neutralized by the adsorbed surfactant ions, the electrostatic attraction is no longer operative and adsorption takes place due to lateral attraction alone with a reduced slope.

d. When the surfactant concentration reaches critical micelle concentration, the surfactant monomer activity becomes constant and any further increase in concentration contributes only to the micellization in solution and it does not change the adsorption density. The adsorption in this region is mainly through lateral hydrophobic interaction between the hydrocarbon chains.

In steps c and d, surfactant molecules adsorb with a reversed orientation (head groups facing the bulk solution) resulting in a decrease in the hydrophobicity of the particles in this region.

pH plays a very significant role in controlling adsorption of ionic surfactants. Thus the adsorption of anionic surfactants is higher on positively charged surfaces [pH below isoelectric point (IEP)] than on negatively charged surfaces while the cationic surfactants adsorb more on negatively charged surfaces [65, 66]. Molecular structure of surfactant does influence its adsorption behavior markedly.

Several adsorption isotherms were assessed and the Langmuir adsorption isotherm was found to be the best description of the adsorption behavior of the investigated surfactants which obeys the following equations:

$$\frac{C_{\text{inh}}}{\theta} = \frac{1}{K} + C_{\text{inh}} \quad (9)$$

where C_{inh} is the inhibitor concentration, θ is the fraction of the surface coverage, K is the modified adsorption equilibrium constant which can be related to the free energy of adsorption ($\Delta G_{\text{ads}}^{\circ}$) as follows:

$$K = \frac{1}{C_{\text{solvent}}} \exp\left(\frac{-\Delta G_{\text{ads}}^{\circ}}{RT}\right) \quad (10)$$

C_{solvent} is the molar concentration of solvent which in the case of the water is 55.5 mol L^{-1} .

Figure 6 shows that the dependence of the fraction of the surface coverage (C/Θ) as a function of the concentration (C) of CTAB and DTAC.

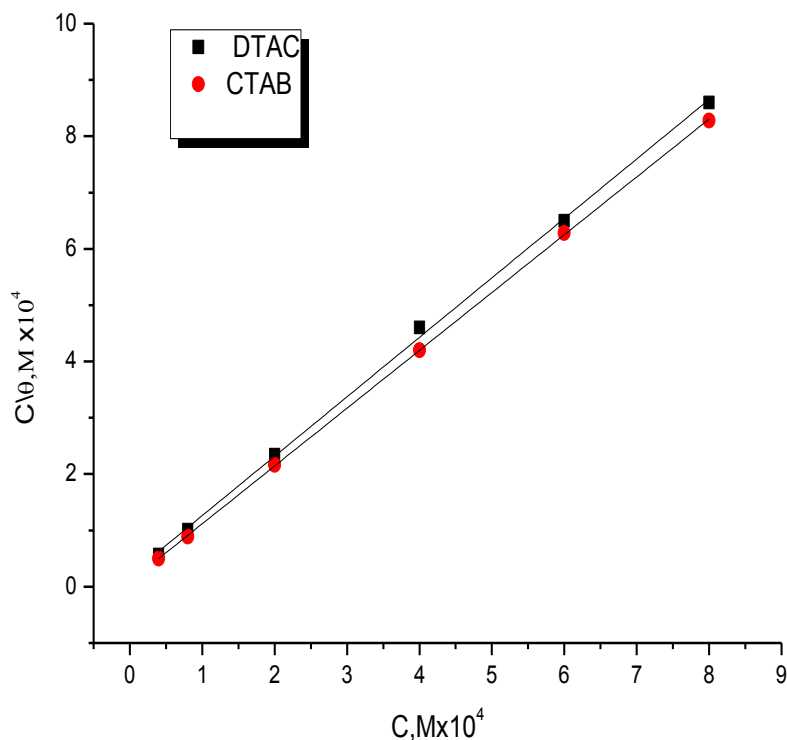


Figure 6. Langmuir adsorption plots for C-steel in 0.5 M HCl containing various concentrations of surfactants

Table 6. Parameters of Langmuir adsorption isotherm

Inhibitor	Temp., K	Adsorption isotherm	$K \times 10^{-4}, \text{ M}^{-1}$	slope	$-\Delta G^{\circ}_{\text{ads}}, \text{ kJ mol}^{-1}$	R^2
DTAC	303	Langmuir	4.88	1.02	37.3	0.999
CTAB			10.30	1.00	39.2	0.999

Therefore, $\Delta G^{\circ}_{\text{ads}}$ can be calculated according to equation (10). The degrees of surface coverage (Θ) were evaluated from weight loss measurements using Eq. 2 and are given in Table 2. The regression coefficient $R^2 = 0.999$ suggests a good relation between C/Θ and C . The values of $\Delta G^{\circ}_{\text{ads}}$ recorded in Table 6 are negative, suggesting the spontaneity of the adsorption process. It is well known that values of $\Delta G^{\circ}_{\text{ads}}$ order of 20 kJ mol^{-1} or lower indicate a physisorption, while those of order of 40 kJ mol^{-1} or higher involve charge sharing or charge transfer from the inhibitor molecules to the metal surface to form a coordinate type of bond (chemisorption) [67, 68]. The calculated values of $\Delta G^{\circ}_{\text{ads}}$ for CTAB are around $-39.9 \text{ kJ mol}^{-1}$, and for DTAC approximately $-39.8 \text{ kJ mol}^{-1}$. It suggests a comprehensive adsorption (physical and chemical adsorption) might be occur [69].

3.3. Computational study

Lower values of ionization potential "I_P" (-E_{HOMO}) are likely to indicate a tendency of the molecule to donate electrons to appropriate acceptor molecules with low energy or empty electron orbital. The higher the values of electron affinity "E_A" (-E_{LUMO}) are, the stronger the electron accepting abilities of the molecules. On the other hand, the hydrophobic properties of the long hydrocarbon tail could be associated with the formation of a protective film that reduces drastically the corrosion process [70].

Pearson introduced the quantities of electronic hardness (η) and softness (σ) in his hard–soft–acid–base principle [71] (HSAB) in the early stage of the reactivity theory. The species are classified as soft (hard) if their valence electrons are easy (hard) to polarize or to remove and the relationship between hardness or softness and the chemical reactivity was given through the HSAB principle, A soft base will interact favorably with a soft acid, sharing electrons, to form bonds of covalent character. Hard acids prefer hard bases and form bonds dominated by electrostatic forces, or ionic character. The concepts of electronegativity (χ) [72] and global hardness (η) [73, 74] are given by:

$$\chi = -\mu = -\left(\frac{\partial E}{\partial N}\right)_{v(r)} \quad (11)$$

$$\eta = \frac{1}{2} \left(\frac{\partial^2 E}{\partial N^2}\right)_{v(r)} = \frac{1}{2} \left(\frac{\partial \mu}{\partial N}\right)_{v(r)} \quad (12)$$

Where μ is the chemical potential, E is the total energy, N is the number of electrons, and $v(r)$ is the external potential of the system.

The global hardness (η), softness (σ), and chemical potential (μ) were calculated in terms of I_P and E_A [75] from the following equations:

$$\eta = \frac{I_P - E_A}{2} \quad (13)$$

$$\sigma = \frac{1}{\eta} = \frac{2}{I_P - E_A} \quad (14)$$

$$\mu = -\frac{I_P + E_A}{2} \quad (15)$$

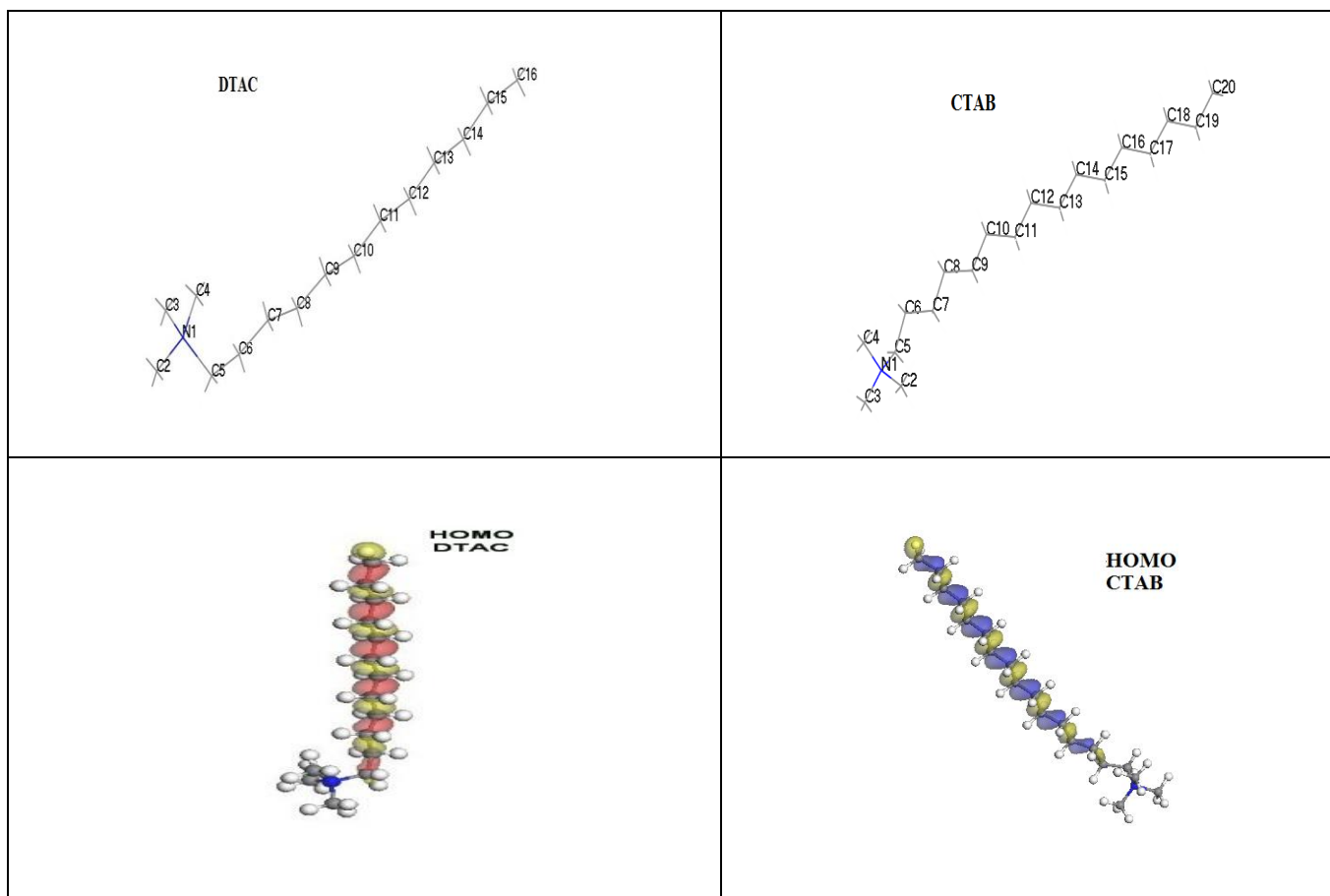
Table 7 shows the quantum chemical calculation parameters obtained by DFT method. The results for the above calculations in gaseous phase as well as in liquid phase are presented. These parameters are mainly ionization potential (I_P), electron affinity (E_A), energy gap (ΔE), global hardness (η), softness (σ), chemical potential (μ) and total energy (E_{tot}). From these results, CTAB exhibits the lowest value of global hardness. It means that this one has a higher reactivity than DTAC, and it is

expected to have the highest corrosion inhibition than DTAC. This expectation is in a good agreement with the experimental results. From Fig.7 we can observed that:

The HOMO location in cationic part of CTAB and DTAC surfactant is mostly distributed on hydrophobic part. The LUMO location in cationic part of CTAB and DTAC is mostly distributed on the head group ions that the preferred sites for the nucleophilic attack through metallic negative centers. The position of the surfactant (lying vertically) could be the reason for the high inhibitor efficiency.

Table 7. Quantum-chemical descriptors for cationic surfactants obtained with DFT meted

		Quantum-chemical descriptors									
			I_p , eV	E_A ,	ΔE ,	η ,	μ ,	σ ,	χ ,	$-E_{tot}$,	
Surfactant	DTAC	Cationic part	Gas phase	8.158	2.934	5.224	2.612	0.383	-5.546	5.546	646.3
			Liquid phase	6.700	-	7.495	3.748	0.267	-2.952	2.952	646.4
		Cl ⁻	Gas phase	-2.33	-	16.75	8.375	0.119	10.705	-5.35	460.23
		counter	Liquid phase	4.53	-	16.75	8.375	0.119	3.85	-3.85	460.35
	CTAB	Cationic part	Gas phase	7.761	3.424	4.337	2.169	0.461	-5.593	5.593	803.6
			Liquid phase	6.569	-	7.316	3.658	0.273	-2.911	2.911	803.69
		Br ⁻	Gas phase	-1.78	-	13.26	6.63	0.151	8.41	-8.41	343.94
		counter	Liquid phase	4.70	-8.54	13.24	6.62	0.151	1.92	-1.92	344.06



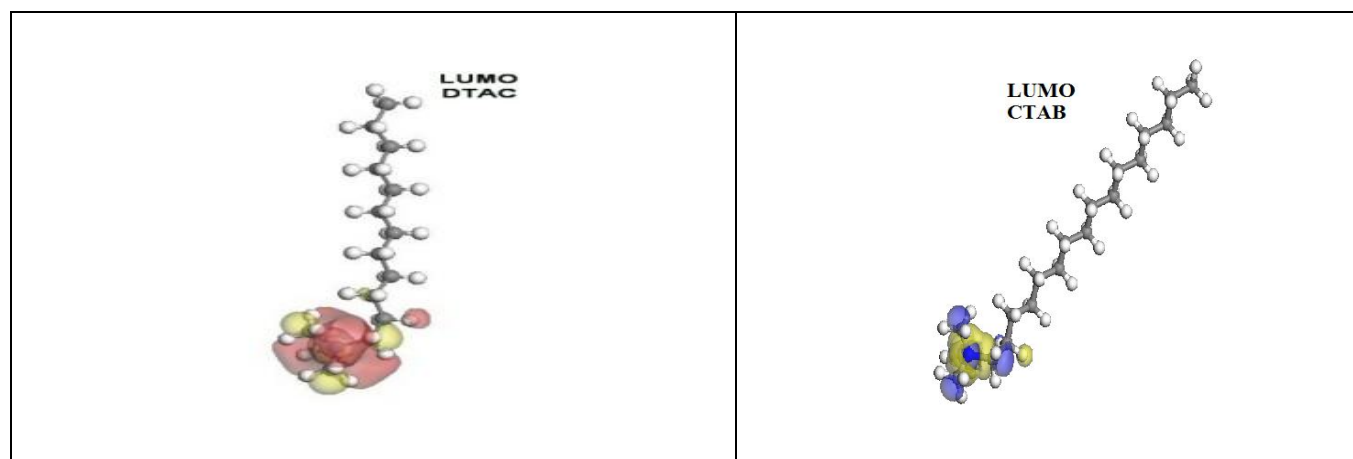


Figure 7. Molecular orbital plots as well as the active sites for electrophilic and nucleophilic attack for DTAC and CTAB respectively.

Table 8. The highest Fukui indices values for the surfactants by Hirshfeld methods in liquid phase calculated with BOP/DNP basis set

DTAC			CTAB		
	Liquid phase			Liquid phase	
	$f^-(r)$	$f^+(r)$		$f^-(r)$	$f^+(r)$
N1	0.000	0.034	N1	-0.003	0.036
C2	0.001	0.077	C2	-0.001	0.061
C3	0.000	0.054	C3	0.001	0.077
C4	0.001	0.062	C4	0.002	0.053
C5	0.007	0.059	C5	0.004	0.058
C6	0.012	0.018	C6	0.006	0.018
C7	0.020	0.009	C7	0.011	0.008
C8	0.032	0.005	C8	0.017	0.006
C9	0.041	0.002	C9	0.024	0.002
C10	0.052	0.001	C10	0.032	0.001
C11	0.054	0.000	C11	0.038	0.000
C12	0.057	0.000	C12	0.044	0.000
C13	0.051	0.000	C13	0.046	0.000
C14	0.046	0.000	C14	0.047	0.000
C15	0.035	0.000	C15	0.045	0.000
C16	0.029	0.000	C16	0.042	-0.001
			C17	0.034	0.000
			C18	0.029	-0.001

Among the theoretical models proposed to compute local reactivity indices is Fukui functions that makes possible to rationalize the reactivity of individual molecular orbital contributions thus to account for the response of the whole molecular spectrum and not only of the frontier orbitals. Frontier orbital electron densities on atoms provide a useful means for the detailed characterization of donor–acceptor interactions. In the case of a donor molecule, $f^-(r)$ electrophilic electron density corresponds to reactivity with respect to electrophilic attack or when the molecule loss electrons and in the case of

an acceptor molecule, $f^+(r)$ nucleophilic electron density corresponds to reactivity with respect to nucleophilic attack. However, frontier electron densities can strictly be used only to describe the reactivity of different atoms in the same molecule.

The highest FI values are presented in Table 8. The most susceptible sites for electrophilic attack located on C(13),C(14) and C(15) atoms in case of CTAB, C(10),C(11),C(12)and C(13) atoms in case of DTAC .In addition, susceptible sites are observed to be attacked by anions or nucleophilic attack, positioned on C(2),C(3),C(4),C(5) and N(1) of CTAB and DTAC.

3.4. Mechanism of Corrosion Inhibition

The role of the counter ions on the adsorption of ionic surfactants is important factor. The feasible adsorption of organic cations in the presence of the halide ions is due to the formation of intermediate bridge, the negative ends of the halide metal dipoles being oriented towards the solution, whereby setting up an additional potential difference between the metal and the solution. This will shift the zero charge potential positively.

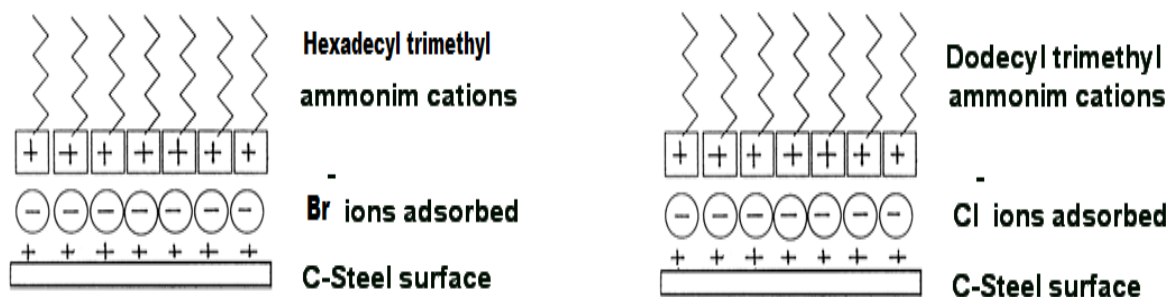


Figure 8. The expected scheme of adsorption of CTAB and DATC inhibitor on C-steel surface

This shift will make the charge on the metal surface more negative and facilitates the adsorption of positively charged quaternary ammonium compound by formation of ionic bonds. High hardness of Br^- ions and Cl^- ions (counter ion effect) and cationic part of CTAB and DTAC suggested higher tendency of an electrostatic adsorption of CTAB and DTAC to occur (Cooperative effect) leads to a high inhibition percentage. Br^- and Cl^- ions act as an adsorption mediator for bonding the two positive partners, the metal surface and the positively charged ammonium compound. This gives rise to the formation of an adsorption composite film in which the anions are sandwiched between the metal and positively charged part of the inhibitor [76]. This film acts as a barrier facing the corrosion process as shown in Fig.8. From above, it is mentioned that a hydrophilic metal surface attracts a large hydrophilic head group of chosen surfactants. Inhibition efficiency of CTAB is larger than DTAC may be due to:

1. Br^- is a borderline base attached with a borderline acid (Fe^{+2} surfaces) and soft acid (bulk Fe metal surfaces) more than the harder Cl^- according to Pearson classification of acids and bases.

2. The alkyl chain of CTAB is longer than DTAC. The greater will be the forces of attraction between the alkyl chains of adjacently adsorbed head group ions [77].

3. Br⁻ ions are more hydrophobic, with large ionic radius and low electronegativity, compared to Cl⁻ [78,79]. Thus it adsorbed more tightly on carbon steel surfaces than Cl⁻ ions.

4. CONCLUSIONS

- The investigated surfactants inhibit the corrosion of C-steel in 0.5 M HCl.
- The inhibition is due to adsorption of the surfactant molecules on the C-steel surface and blocking its active sites.
- Adsorption of the investigated surfactants fits a Langmuir isotherm model.
- Results obtained from weight loss, dc polarization, ac impedance and EFM techniques are in reasonably good agreement and show increased inhibitor efficiency with increasing inhibitor concentration.
- Polarization data shows that the investigated surfactants act as mixed-type inhibitor in 0.5 M HCl.
- The theoretical study of molecules indicated the difference between CTAB and DTAC according to HSAB principle.

References

1. J.E. Oddo, M.B. Tomson, *J. Pet. Tech.* (1982) 1583.
2. B. Ridd, T.J. Blakset, D. Queen, Corrosion, NACE, Paper No (78), Houston, Texas, 1998.
3. J.M. Bastidas, P. Pinilla, J.L. Polo, S. Miguel, *Corros. Sci.* 45 (2003) 427–449.
4. A.E. Bolzán, I.B. Wakenge, R.C.V. Piatti, R.C. Salvarezza, A.J. Arvia, *J. Electroanal. Chem.* 501 (2001) 241–252.
5. E. Stipnisek-Lisac, A. Gazivoda, M. Madzarac, *Electrochim. Acta* 47 (2002) 4189–4194.
6. M. Sahin, S. Bilgic, H. Yilmaz, *Appl. Surf. Sci.* 195 (2002) 1–7.
7. H. Luo, Y.C. Guan, K.N. Han, *Corrosion* 54 (1998) 619–627.
8. C.A. Miller, S. Qutubuddin, in: H.F. Eick, C.D. Parfitt (Eds.), *Interfacial Phenomena in Apolar Media*, Surfactant Science Series, vol. 21, Markel Dekker Inc., New York, Basel, 1987, p. 166.
9. O. Olivares, N.V. Likhanova, B. Gomez, J. Navarrete, M.E. Llanos-Serrano, E. Arce, J.M. Hallen, *Appl. Surf. Sci.*, 252 (2006) 2894.
10. S. Trasatti, *Electrochim. Acta*, 37 (1992) 2137.
11. A. Popova, E. Sokolova, S. Raicheva, M. Christov, *Corros. Sci.*, 45 (2003) 33.
12. N. Hajjaji, I. Ricco, A. Srhiri, A. Lattes, M. Soufiaoui, A. Ben Bachir, *Corrosion* 49(1993)326
13. M. Elachouri, M.S. Hajji, M. Salem, S. Kertit, R. Coudert, E.M. Essassi, *Corros Sci* 37(1995)381
14. H. Luo, Y.C. Guan, K.N. Han, *Corrosion* 54(1998)619
15. M.A. Migahed, E.M.S. Azzam, A.M. Al-Sabagh, *Mater Chem Phys* 85(2004)273
16. M.M. Osman, A.M. Omar, A.M. Al-Sabagh, *Mater Chem Phys* 50(1997)271
17. F. Zucchi, G. Trabanelli, G. Brunoro, *Corros Sci* 33(1992)1135
18. M. Elachouri, M.S. Hajji, S. Kertit, E.M. Essassi, M. Salem, R. Coudert, *Corros Sci* 37(1994)381
19. Z. Wei, P. Duby, P. Somasundaran, *J Colloid Interface Sci* 259(2003)97
20. J.M. Bastidas, J.L. Polo, E. Cano, C.L. Torre, *J Mat Sci* 35(2000)2637

21. J.M.Bastidas, J.L.Polo, E.Cano, *J Appl Electrochem*30(2000)1173
22. Z.Abdel Hamid, T.Y.Soror, H.A.El Dahan, A.M.Omar, *Anti-Corros Methods Mater* 45(1998) 306
23. M. Saleh, A.A.Atia, *J Appl Electrochem* 36(2006)899
24. M.A.Migahed, *Mater Chem Phys* 93(2005)48
25. A.M.Al Sabagh, M.A. Migahed, H.S.Awad HS *Corros Sci*48(2006) 813
26. A.K.Maayta, M.B.Bitara, M.M.Al-Abdallah, *Br Corros J* 36(2001)133
27. R.V.F.Villamil, P.Corio, J.C.Rubim, M.L.Silvia Agostinho, *J Electroanal Chem* 472(1999)112
28. R. Fuchs-Godec, V.Dolecek, *Colloids Surf A* 244(2004)73
29. H. Ma, S. Chen, B. Yin, S. Zhao, X. Liu, *Corros Sci* 45(2003)867
30. A.A. Amin, *J Appl Electrochem* 36(2006)215
31. D.Q. Zhan, L.X.Gao, G.D. Zhou, K.Y. Lee, *J Appl Electrochem*38(2008) 71
32. T.P. Zhao, G.N. Mu, *Corros Sci* 41(1999) 1937
33. S.S. Abd El Rehim, H.H. Hassaan, M.A. Amin, *Mater ChemPhys* 70(2001) 64
34. S.S. Abd El Rehim, H.H. Hassaan, M.A. Amin, *Mater ChemPhys* 78(2002) 337
35. A.K. Maayta, N.A.F. Al-Rawashdeh, *Corros Sci* 46(2004) 1129
36. R. Guo, T. Liu, X. Wei, *Colloids Surf A* 209(2002) 37
37. V. Branzoi, F. Golgovici, F. Branzoi, *Mater Chem Phys* 78(2002) 122
38. L.G. Qiu, A.J. Xie, Y.H. Shen, *Corros. Sci.* 47 (2005) 273–278.
39. M. El Achouri, M.R. Infante, F. Izquierdo, S. Kertit, H.M. Gouytaya, B. Nciri, *Corros. Sci.* 43 (2001) 19–35.
40. D. Asefi, M. Arami, N.M. Mahmoodi, *Corros. Sci.* 52 (2010) 794–800.
41. X. Wang, H. Yang, F. Wang, *Corros. Sci.* 52 (2010) 1268–1276.
42. L.-G. Qiu, Y. Wu, Y.-M. Wang, X. Jiang, *Corros. Sci.* 50 (2008) 576–582.
43. S.-Z. Yao, X.-H. Jiang, L.-M. Zhou, Y.-J. Lv, X.-Q. Hu, *Mater. Chem. Phys.* 104(2007) 301–305.
44. M.A. Hegazy, *Corros. Sci.*, 51 (2009) 2610–2618.
45. VoltMaster 4 Manual, 2000.
46. B. Delley, *J. Chem. Phys.*, 92 (1990) 508.
47. B. Delley, *J. Chem. Phys.*, 113 (2000) 7756.
48. R.S. Mulliken, *J. Chem. Phys.*, 23 (1995) 1833.
49. H. Ma, S. Chen, B. Yin, S. Zhao, X. Liu, *Corros. Sci.*, 45 (2003)867-882.
50. C.N. Cao, Corrosion Electrochemistry Mechanism, Chemical Industrial Engineering Press, Beijing, (in Chinese), (2004) 325.
51. M. El Achouri, S. Kertit, H.M. Gouytaya, B. Nciri, Y. Bensouda, L. Perez, M.R. Infante, K. Elkacemi, *Prog. Org. Coat.*, 43 (2001) 267.
52. K.F. Khaled, *Electrochim. Acta*, 48 (2003) 2493.
53. A.Popova, E. Sokolova, S. Raicheva, M. Christov, *Corros. Sci.* 45 (2003) 33
54. F.B. Growcock, J.H. Jasinski, *J. Electrochem. Soc.*, 136 (1989) 2310
55. U. Rammet, G. Reinhart, *Corros. Sci.*, 27 (1987) 373.
56. A.H. Mehaute, G. Grep, *Solid State Ionics* 9–10 (1983) 17.
57. E. Machnikova, M. Pazderova, M. Bazzouai, N. Hackerman, *Surf. Coat. Technol.*202 (2008) 1543.
58. C.H. Hsu, F. Mansfeld, *Corrosion*, 57 (2001) 747.
59. M. Lebrini, M. Lagrenée, M. Traisnel, L. Gengembre, H. Vezin, F. Bentiss, *Appl. Surf. Sci.*, 253 (2007) 9267
60. R.G. Kelly, J.R. Scully, D.W. Shoesmith, R.G. Buchheit, *Electrochemical Techniques in Corrosion Science and Engineering*, Marcel Dekker, Inc., New York, 2002. p. 148.
61. Gamry Echem Analyst Manual, 2003.
62. R.W. Bosch, J. Hubrecht, W.F. Bogaerts, B.C. Syrett, *Corrosion*, 57 (2001) 60.
63. Somasundaran P, Grieves RB, editors. *Advances in interfacial phenomena* of Marcel Dekker, 1988.

64. D.T.Wasan, M.Ginn, D.O.Shah, Surfactants in process engineering, New York, particulate/solution/gas systems. AIChE Symposium Series, 1975; 71 AIChE Symp. Ser. 71 (1975) 124
65. Fuerstenau DW. The adsorption of surfactants at solid/water interfaces. In: Hair ML, editor. The chemistry of biosurfaces, vol. New York: Marcel Dekker; 1971. p. 143
66. L. Koopal, E. Lee, M. Böhmer. *J Colloid Interface Sci.*, 170 (1995) 85.
67. A.X.Fan, P. Somasundaran, and N.J. Turro, *Langmuir*, 13 (1997) 506.
68. F.M. Donahue, K. Nobe, *J. Electrochem. Soc.*, 112 (1965) 886.
69. E. Khamis, F. Belluci, R.M. Latanision, E.S.H. El-Ashry, *Corrosion*, 47 (1991) 677.
70. A.K.Singh, M.A.Quraishi, *Corros.Sci.*, 52 (2010)1378.
71. D.A. Lopez, S.N. Simison, S.R. de Sa'nchez, *Corros. Sci.*, 47 (2005) 735
72. R.G. Pearson, *J. Am. Chem. Soc.*, 85 (1963) 3533
73. R.G. Parr, D.A. Donnelly, M. Levy, M. Palke, *J. Chem. Phys.*, 68 (1978) 3801.
74. R.G. Parr, R.G. Pearson, *J. Am. Chem. Soc.*, 105 (1983) 7512.
75. R.G. Pearson, *Inorg. Chem.*, 27 (1988) 734.
76. V.S. Sastri, J.R. Perumareddi, *Corros. Sci.*, 53 (1997) 617
77. T.Y. Soror, M.A. El-Ziady, *Mater. Chem. Phys.*, 77 (2002) 702.
78. V. Branzoi, F. Branzoi, M. Biabarac, *Mater. Chem. Phys.*, 65(2000)294.
79. E.E. Oguzie, G.N. Onuoha, A.I. Onuchukwu, *Mater. Chem. Phys.*, 89(2004) 305.
80. Y.I. Kuznetsov, N.N. Andreev, Corrosion (NACE) International, Houston, paper No. 214 (1996)